Chinese Chemical Letters 35 (2024) 108953

Contents lists available at ScienceDirect

Chinese Chemical Letters

journal homepage: www.elsevier.com/locate/cclet

Demethylase-assisted site-specific detection of N^1-methyladenosine in RNA

Jun Xiong[a,1], Ke-Ke Chen[a,1], Neng-Bin Xie[a,1], Wei Chen[b,1], Wen-Xuan Shao[a], Tong-Tong Ji[a], Si-Yu Yu[a], Yu-Qi Feng[a], Bi-Feng Yuan[a,*]

[a] College of Chemistry and Molecular Sciences, Research Center of Public Health, Renmin Hospital of Wuhan University, School of Public Health, Wuhan University, Wuhan 430071, China
[b] Department of Laboratory Medicine, Zhongnan Hospital of Wuhan University, Wuhan University, Wuhan 430071, China

ARTICLE INFO

Article history:
Received 15 May 2023
Revised 7 August 2023
Accepted 21 August 2023
Available online 24 August 2023

Keywords:
N^1-methyladenosine
RNA modification
AlkB demethylase
RNA epigenetics
Quantitative real-time PCR
Hepatocellular carcinoma

ABSTRACT

The dynamic RNA modifications have been viewed as new posttranscriptional regulator in modulating gene expression as well as in a broad range of physiological processes. N^1-methyladenosine (m^1A) is one of the most prevalent modifications existing in multiple types of RNAs. In-depth investigation of the functions of m^1A requires the site-specific assessment of m^1A stoichiometry in RNA. Herein, we established a demethylase-assisted method (DA-m^1A) for the site-specific detection and quantification of m^1A in RNA. *N*1-methyl group in m^1A could result in the stalling of reverse transcription at m^1A site, thus producing the truncated cDNA. *E. coli* AlkB is a demethylase that can demethylate m^1A to produce adenine in RNA, thus generating full-length cDNA from AlkB-treated RNA. Evaluation of the produced amounts of full-length cDNA by quantitative real-time PCR can achieve the site-specific detection and quantification of m^1A in RNA. With the DA-m^1A method, we examined and successfully confirmed the previously well-characterized m^1A sites in various types of RNAs with low false positive rate. In addition, we found that the level of m^1A was significantly decreased at the bromodomain containing 2 (*BRD2*) mRNA position 1674 and CST telomere replication complex component 1 (*CTC1*) mRNA position 5643 in human hepatocellular carcinoma tissues. The results suggest that these two m^1A sites in mRNA may be involved in liver tumorigenesis. Taken together, the DA-m^1A method is simple and enables the rapid, cost-effective, and site-specific detection and quantification of m^1A in RNA, which provides a valuable tool to decipher the functions of m^1A in human diseases.

In addition to the four canonical nucleosides of adenosine (A), guanosine (G), cytidine (C) and uridine (U), RNA molecules also contain diverse chemical modifications [1–3]. Since the first modification was characterized over 60 years ago, more than 150 chemical modifications have been identified in a variety of RNA species from three-domain of life [4–8]. RNA modifications occur in ribosomal RNA (rRNA), transfer RNA (tRNA), messenger RNA (mRNA), and non-coding RNAs (ncRNAs) [9–11]. Similar to epigenetic DNA methylation, RNA modifications have their own writers, erasers, and readers [12,13]. Now, the dynamic RNA modifications have been viewed as new posttranscriptional regulator in modulating gene expression as well as in a broad range of physiological processes [14–19].

N^6-methyladenosine (m^6A) is the best-characterized internal modification in eukaryotic mRNA [20]. As an isomer of m^6A, N^1-methyladenosine (m^1A) has also been found to be present in all the three kingdoms of life [21]. m^1A is a reversible modification occurring in tRNA, rRNA, mRNA, and mitochondrial RNA [22,23]. The methyl group in m^1A could disturb the formation of the Watson–Crick base pair (Fig. 1A), which would therefore affect the secondary structure of RNA and the interaction with its reader proteins. It has been reported that m^1A is involved in the folding of tRNA [24–26], maturation of ribosomes [27], and translation process [28,29].

In recent years, mass spectrometry-based and sequencing-based techniques have been developed to discover, identify, and map nucleic acid modifications [30–37]. The presence of *N*1-methyl group in m^1A could induce stop or misincorporation feature in reverse transcription (RT), which was employed for the transcriptome-wide mapping of m^1A while in combination with high-throughput sequencing [28,29]. However, these high-

* Corresponding author.
E-mail address: bfyuan@whu.edu.cn (B.-F. Yuan).
[1] These authors contributed equally to this work.

https://doi.org/10.1016/j.cclet.2023.108953
1001-8417/

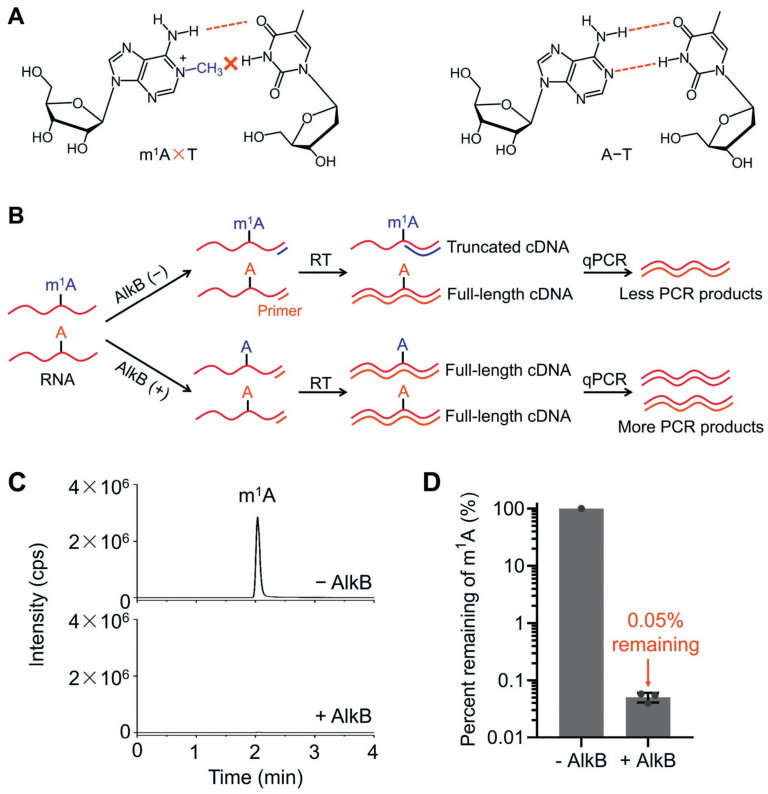

Fig. 1. Schematic illustration of the principle of DA-m^{1}A method. (A) *N*1-methyl group in m^{1}A can disturb the formation of hydrogen bonding between m^{1}A and thymine, while adenosine and thymine can form classic Watson–Crick base pairing. (B) In DA-m^{1}A method, m^{1}A in RNA will cause RT stalling in m^{1}A, producing truncated cDNA. Removal of m^{1}A by AlkB will lead to the generation of full-length cDNA. Evaluation of the produced amounts of full-length cDNA by qPCR could realize site-specific detection and quantification of m^{1}A in RNA. (C, D) LC-MS/MS analysis of the demethylation efficiency toward m^{1}A by AlkB treatment. Error bars indicate mean ± SD with three replicates.

throughput sequencing-based methods generally require complex sample pretreatment and sequencing library construction, which is time-consuming, costly and needs sophisticated bioinformatics analysis. Mass spectrometry-based analysis generally offers the identification and quantification of bulky RNA modifications [38–40]. However, the site information of RNA modifications typically couldn't be obtained by mass spectrometry-based methods. Some studies aim to evaluate m^{1}A at certain critical sites with stoichiometry information. In this respect, a method that enables rapid, straightforward, site-specific detection and quantification of m^{1}A is highly desired. m^{1}A carries a methyl group in the *N*1 position of adenine, which can compromise the formation of hydrogen bonding between m^{1}A and thymine (Fig. 1A). By virtue of this property of m^{1}A, we developed a demethylase-assisted method (DA-m^{1}A) for the site-specific assessment of m^{1}A stoichiometry in RNA. The presence *N*1-methyl group in m^{1}A could cause the stalling of reverse transcription at m^{1}A site, thus producing the truncated cDNA. *E. coli* AlkB is a demethylase that acts as a repair protein and can demethylate m^{1}A [41,42]. Since m^{1}A can cause the stalling of reverse transcription and produce truncated cDNA in RT reaction, we envisioned that AlkB-assisted demethylation of m^{1}A to produce adenine in RNA would generate full-length cDNA. Therefore, evaluation of the produced amounts of full-length cDNA by qPCR could realize site-specific detection and quantification of m^{1}A in RNA (Fig. 1B).

We first expressed and purified the recombinant AlkB protein (Table S1, Figs. S1 and S2 in Supporting information). We employed LC-MS/MS to evaluate the demethylation efficiency of m^{1}A by AlkB protein (Table S2 in Supporting information). Since the bromodomain containing 2 (*BRD2*) mRNA was proved to contain m^{1}A at position 1674 [43], a 46-nt RNA (Oligo-m^{1}A, Table S3 in Supporting information) that has the same sequence context around the position 1674 of *BRD2* mRNA was synthesized and used as the substrate for the evaluation. Oligo-m^{1}A was treated with AlkB followed by enzymatic digestion and LC-MS/MS analysis. The result showed that m^{1}A was almost undetectable after AlkB treatment (Fig. 1C). Quantification of the trace level of m^{1}A demonstrated that 99.95% demethylation efficiency toward m^{1}A was achieved upon AlkB treatment (Fig. 1D). The highly efficient demethylation of m^{1}A by AlkB indicates the high feasibility for the development of the DA-m^{1}A method.

Two 46-nt RNAs of Oligo-m^{1}A and Oligo-A (Table S3) were used as the templates for the optimization reaction. A 78-nt DNA (Preamp oligo) was designed to hybridize with Oligo-m^{1}A and Oligo-A for the RT reaction. The RT stalling efficiencies were calculated using the equation of $\Delta Ct = Ct_{m1A} - Ct_A$ (Figs. 2A and B).

Based on the ΔCt values, we first evaluated the RT stalling efficiency of m^{1}A by five commercial reverse transcriptases, including ProtoScript II reverse transcriptase, *Bst* 3.0 DNA polymerase, SuperScript III reverse transcriptase, M-MuLV reverse transcriptase, and AMV reverse transcriptase. The results showed that larger ΔCt values were obtained with using ProtoScript II reverse transcriptase and *Bst* 3.0 DNA polymerase, indicating m^{1}A would lead to stronger RT stalling by these two transcriptases (Fig. 2C). We then optimized the reaction temperatures of these five reverse transcriptases from 37 °C to 70 °C. The results showed that ProtoScript II reverse transcriptase exhibited overall the best discrimination between m^{1}A and A under the temperature ranging from 37 °C to 52 °C (Fig. 2C). Similar to the qPCR results, the PAGE analysis also suggested that m^{1}A exhibited stronger RT stalling efficiency with using Protoscript II reverse transcriptase (Fig. 2D). As expected, the band intensities from the AlkB-treated Oligo-m^{1}A template were

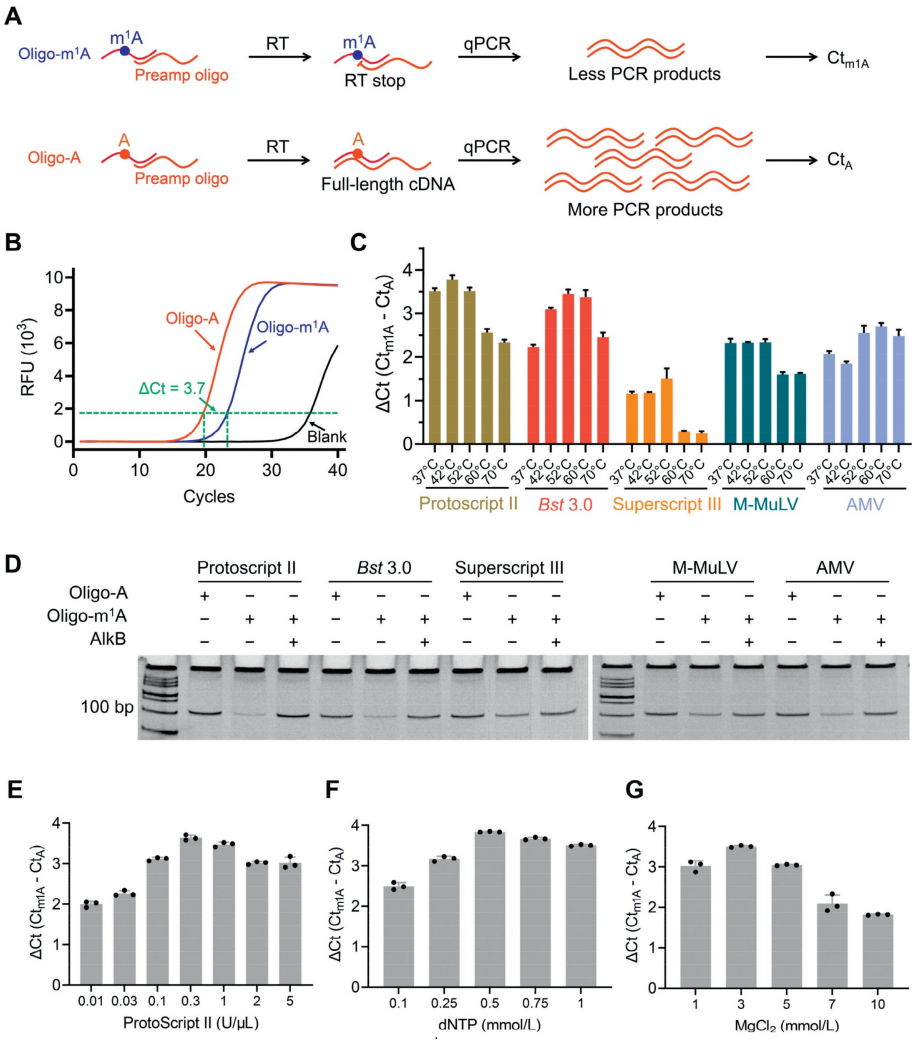

Fig. 2. Optimization of the RT reaction in DA-m^{1}A method. (A) Schematic illustration showing that differential Ct values could be obtained from Oligo-m^{1}A (Ct_{m1A}) and Oligo-A (Ct_A) in DA-m^{1}A method. The ΔCt (Ct_{m1A}-Ct_A) values are used to evaluate the RT stalling efficiency. (B) Representative real-time fluorescence amplification curves with using Oligo-m^{1}A and Oligo-A templates. (C) Evaluation of the RT stalling efficiencies by different reverse transcriptases under different temperatures. (D) Evaluation of the RT stalling efficiencies by different reverse transcriptases with PAGE analysis. 22 cycles were carried out for PCR. (E–G) Optimization of the concentrations of Protoscript II reverse transcriptase, dNTP, and Mg^{2+}. Error bars indicate mean ± SD with three replicates.

comparable to the Oligo-A template, indicating that AlkB treatment would efficiently remove the methyl group of m^{1}A and therefore eliminate the RT stalling caused by m^{1}A (Fig. 2D).

Since ProtoScript II reverse transcriptase shows the best performance in discriminating m^{1}A and A under 42 °C (Fig. 2C), we chose this enzyme for the method development. To obtain the best discrimination, we further optimized the conditions of the RT reactions, including the concentrations of Protoscript II reverse transcriptase, dNTP, and Mg^{2+}. With the increased concentration of Protoscript II reverse transcriptase, the ΔCt values increased and slightly decreased over 0.3 U/μL (Fig. 2E). The concentrations of dNTP and Mg^{2+}also affected the discrimination between m^{1}A and A. The results showed that 0.5 mmol/L dNTP and 3 mmol/L Mg^{2+} offered the best discrimination (Figs. 2F and G). Collectively, the optimal RT reaction was conducted under 42 °C with 0.5 mmol/L dNTP, 3 mmol/L $MgCl_2$ and 0.3 U/μL Protoscript II reverse transcriptase.

Having optimized the conditions of the DA-m^{1}A method, we evaluated its quantitative ability toward m^{1}A at given sites in RNA. We first constructed a calibration curve using different concentrations of Oligo-A and Oligo-m^{1}A from 10^{-15} mol/L to 10^{-9} mol/L (Fig. S3 in Supporting information). The Ct values were plotted against the logarithm (lg) of the concentrations of Oligo-A or Oligo-m^{1}A. The resulting equations of $Ct_A = -3.005\lg C_{Oligo\text{-}A} - 14.681$ and $Ct_{m1A} = -3.028\lg C_{Ologo\text{-}m1A} - 11.360$ showed good linearity with R^2 being 0.997 (Figs. S4A and B in Supporting information). The obtained ΔCt ($Ct_{m1A} - Ct_A$) were similar under different concentrations of Oligo-A and Oligo-m^{1}A (from 10^{-15} mol/L to 10^{-9} mol/L, Fig. S4C in Supporting information), indicating the DA-m^{1}A method can be applied in the detection of m^{1}A with a wide range of concentrations of RNA substrates.

We next quantitatively assessed the m^{1}A level in individual sites by the DA-m^{1}A method. In this respect, the mixtures of Oligo-A and Oligo-m^{1}A with various molar ratios of Oligo-m^{1}A/(Oligo-m^{1}A + Oligo-A) were prepared and subjected to AlkB treatment. The ΔCt (Ct_{AlkB-} – Ct_{AlkB+}) values between untreated mixtures (Ct_{AlkB-}) and AlkB-treated mixtures (Ct_{AlkB-}) were plotted against the theoretical percentages of m^{1}A fraction (Fig. 3A). A non-linear fitting curve ($y = 1.156x/(100 - 0.675x)$) was generated with R^2 being 0.998 (Fig. 3B). With this equation, we quantified the m^{1}A level at specific loci in RNA of HEK293T cells (Fig. S5 in Supporting information). We first examined a control site without m^{1}A modification (position 316) in 28S rRNA. As shown in Fig. S6A (Supporting information), the ΔCt (0.02) was extremely low, indicat-

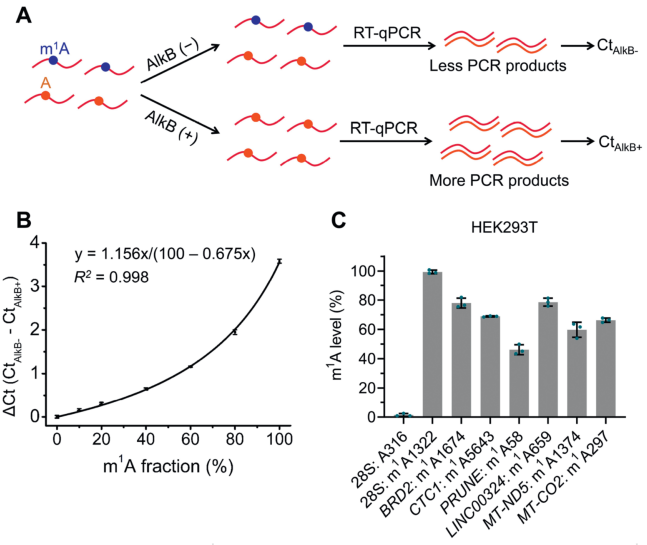

Fig. 3. Assessment of m^{1}A stoichiometry at given sites in RNA by DA-m^{1}A method. (A) Schematic illustration showing the assessment of m^{1}A stoichiometry at given sites in RNA by DA-m^{1}A method. The mixtures of Oligo-A and Oligo-m^{1}A with various molar ratios were prepared and subjected to AlkB treatment. (B) The ΔCt (Ct_{AlkB-} – Ct_{AlkB+}) values between untreated mixtures (Ct_{AlkB-}) and AlkB-treated mixtures (Ct_{AlkB-}) were plotted against the theoretical percentages of m^{1}A fraction. (C) Assessment of m^{1}A stoichiometry at specific loci in RNA of HEK293T cells by DA-m^{1}A method. Error bars indicate mean ± SD with three replicates.

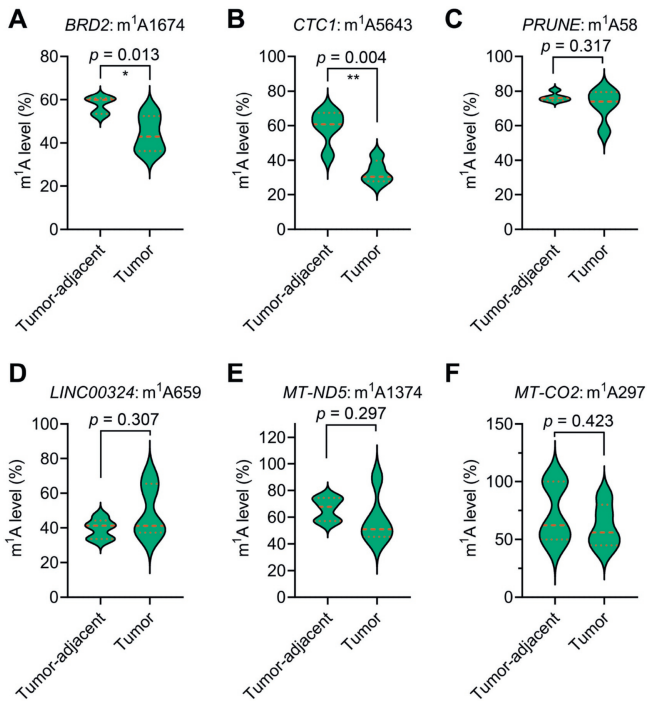

Fig. 4. Site-specific quantification of m^{1}A in RNA of human HCC tissues by DA-m^{1}A method. Total RNA from five pairs of human HCC tissues and their matched tumor-adjacent normal tissues were isolated and subjected to DA-m^{1}A analysis. (A) *BRD2*: m^{1}A1674. (B) *CTC1*: m^{1}A5643. (C) *PRUNE*: m^{1}A58. (D) *LINC00324*: m^{1}A659. (E) *MT-ND5*: m^{1}A1374. (F) *MT-CO2*: m^{1}A297. All *p* values were evaluated by a two-sided paired *t*-test.

ing low false positive rate of the DA-m^{1}A method. We then examined the previously well-characterized m^{1}A site (position 1322) in 28S rRNA [44]. The result showed a ΔCt of 3.49 was obtained, and the m^{1}A level was calculated to be 99.4% ± 1.2% (Fig. 3C and Fig. S6B in Supporting information), which was consistent with the previous study [44]. m^{1}A modification occurs in different RNA species, including mRNA, ncRNA, and mitochondrial RNA [22,23]. We also applied the DA-m^{1}A method to quantify m^{1}A level in individual sites of different RNA species. Some previously reported m^{1}A sites, including *BRD2* mRNA position 1674 (*BRD2*: m^{1}A1674), CST telomere replication complex component 1 (*CTC1*) mRNA position 5643 (*CTC1*: m^{1}A5643), ncRNA prune exopolyphosphatase 1 (*PRUNE1*) position 58 (*PRUNE*: m^{1}A58), long intergenic non-protein coding RNA 324 (*LINC00324*) position 659 (*LINC00324*: m^{1}A659), mitochondrially encoded NADH:ubiquinone oxidoreductase core subunit 5 mRNA (*MT-ND5*: m^{1}A1374) and mitochondrially encoded cytochrome C oxidase II mRNA (*MT-CO2*: m^{1}A297). The measured levels of m^{1}A at *BRD2*: m^{1}A1674, *CTC1*: m^{1}A5643, *PRUNE*: m^{1}A58, *LINC00324*: m^{1}A659, *MT-ND5*: m^{1}A1374, and *MT-CO2*: m^{1}A297 were 77.9% and 68.8%, 46.1%, 78.6%, 59.7%, and 66.3%, respectively (Fig. 3C and Figs. S6C-H in Supporting information). The quantification results of these m^{1}A sites are comparable to previously reported data (91% for *BRD2*: m^{1}A1674, 84% for *CTC1*: m^{1}A5643, 49% for *PRUNE*: m^{1}A58, 82% for *LINC00324*: m^{1}A659, 67% for *MT-ND5*: m^{1}A1374, and 76% for *MT-CO2*: m^{1}A297) [44–46]. Taken together, these results suggest that the DA-m^{1}A method is capable for site-specific assessment of m^{1}A stoichiometry in RNA.

Nucleic acid modifications are known to be involved in a variety of human cancer development [47–49]. It has been reported that m^{1}A in tRNA is elevated in human hepatocellular carcinoma (HCC) tissues and drives liver tumorigenesis [50]. However, site-specific quantification of the change of m^{1}A in RNA of HCC tissues is lacked.

Here we explored the correlation of the levels of m^{1}A at specific sites in RNA with HCC. The total RNA from 5 pairs of human HCC tissues and their matched tumor-adjacent normal tissues were isolated and subjected to DA-m^{1}A analysis (Table S4 in Supporting information). An approval for the study was granted by the Wuhan University Ethics Committee and met the declaration of Helsinki. All experiments were conducted in accordance with Wuhan University Ethics Committee's guidelines and regulations. The aforementioned six m^{1}A sites were evaluated (Tables S5 and S6 in Supporting information). The results showed that, compared to the tumor-adjacent normal tissues, m^{1}A level in HCC tissues was significantly decreased at *BRD2*: m^{1}A1674 ($P = 0.013$) and *CTC1*: m^{1}A5643 ($P = 0.004$) (Figs. 4A and B, Figs. S7A and B in Supporting information). m^{1}A level in the other 4 sites showed no significant change between HCC tissues and tumor-adjacent normal tissues (Figs. 4C–F and Figs. S7C–F in Supporting information). The results suggested that the two m^{1}A sites in mRNA (*BRD2*: m^{1}A1674 and *CTC1*: m^{1}A5643) may be involved in liver tumorigenesis.

LC-MS/MS analysis only could provide the bulky level of m^{1}A, which is not able to accurately reflect the site-specific change of m^{1}A between samples. Indeed, the bulky m^{1}A level in the total RNA measured by LC-MS/MS showed no significant change between human HCC tissues and their matched tumor-adjacent normal tissues (P=0.930, Fig. S8 in Supporting information). Although the bulky m^{1}A level may not have obvious change, the levels of m^{1}A at certain sites may have significant changes between cancer tissues and normal tissues. Since the DA-m^{1}A method enables the site-specific quantification of m^{1}A with stoichiometry information, it allows the evaluation of precise alteration of m^{1}A at given sites. The DA-m^{1}A is a well complementary method to LC-MS/MS method. In addition, the DA-m^{1}A method is also suitable to be employed to confirm the m^{1}A sites determined by transcriptome-wide mapping methods. The limitation of the DA-m^{1}A method is that it relies on prior knowledge of sequence information flanking the target m^{1}A.

In summary, we proposed the DA-m^{1}A method for the site-specific assessment of m^{1}A stoichiometry in RNA from biological

and clinical samples. With the DA-m^{1}A method, we examined and successfully confirmed the previously well-characterized m^{1}A sites in 28S rRNA, mRNA, ncRNA, and mitochondrial RNA with low false positive rate. In addition, we found the level of m^{1}A was significantly decreased at *BRD2* mRNA position 1674 and *CTC1* mRNA position 5643 in human HCC tissues, suggesting that these two m^{1}A sites in mRNA might be involved in liver tumorigenesis. Collectively, the developed DA-m^{1}A method offers a straightforward, cost-effective, and site-specific detection of m^{1}A with stoichiometry. The DA-m^{1}A method is simple and rapid, which is especially suitable for the evaluation of the status of certain critical m^{1}A sites in RNA from a plenty number of biological or clinical samples.

Declaration of competing interest

The authors declare that they have no known competing financial interests or personal relationships that could have appeared to influence the work reported in this paper.

Acknowledgments

The work is supported by the National Key R&D Program of China (Nos. 2022YFC3400700 and 2022YFA0806600), the National Natural Science Foundation of China (Nos. 22277093, 22074110, 21721005 and 22207090), the Interdisciplinary Innovative Talents Foundation from Renmin Hospital of Wuhan University (No. JCRCGW-2022–008), and the Translational Medicine and Interdisciplinary Research Joint Fund of Zhongnan Hospital of Wuhan University (No. ZNJC202208).

Supplementary materials

Supplementary material associated with this article can be found, in the online version, at doi:10.1016/j.cclet.2023.108953.

References

[1] D. Wiener, S. Schwartz, Nat. Rev. Genet. 22 (2021) 119–131.
[2] S. Moshitch-Moshkovitz, D. Dominissini, G. Rechavi, Cell 185 (2022) 764–776.
[3] Y. Zhao, X. Zuo, Q. Li, et al., Sci. China Chem. 64 (2021) 171–203.
[4] P. Boccaletto, F. Stefaniak, A. Ray, et al., Nucleic Acids Res. 50 (2022) D231–D235.
[5] M.Y. Chen, Z. Gui, K.K. Chen, et al., Chin. Chem. Lett. 33 (2022) 2086–2090.
[6] X.J. You, S. Zhang, J.J. Chen, et al., Nucleic Acids Res. 50 (2022) 9858–9872.
[7] Y. Dai, C.B. Qi, Y. Feng, et al., Anal. Chem. 93 (2021) 6938–6946.
[8] M.Y. Cheng, X.J. You, J.H. Ding, et al., Chem. Sci. 12 (2021) 8149–8156.
[9] Y. Motorin, M. Helm, Wiley Interdiscip. Rev. RNA 13 (2022) e1691.
[10] J.H. Ding, M.Y. Chen, N.B. Xie, et al., Biosens. Bioelectron. 219 (2023) 114821.
[11] M.Y. Chen, C.B. Qi, X.M. Tang, et al., Chin. Chem. Lett. 33 (2022) 3772–3776.
[12] T.R. Fischer, L. Meidner, M. Schwickert, et al., Nucleic Acids Res. 50 (2022) 4216–4245.
[13] F. Nie, P. Feng, X. Song, et al., Database 2020 (2020) baaa049.
[14] H.L. Huang, H.Y. Weng, X.L. Deng, J.J. Chen, Annu. Rev. Cancer Biol. 4 (2020) 221–240.
[15] K. Chen, B.S. Zhao, C. He, Cell Chem. Biol. 23 (2016) 74–85.
[16] H. Shi, P. Chai, R. Jia, X. Fan, Mol. Cancer 19 (2020) 78.
[17] M. Frye, B.T. Harada, M. Behm, C. He, Science 361 (2018) 1346–1349.
[18] Y.Y. Chen, Z. Gui, D. Hu, et al., Chin. Chem. Lett. 34 (2023) 108522.
[19] J.J. Chen, X.J. You, L. Li, et al., Anal. Chem. 94 (2022) 8740–8747.
[20] S. Murakami, S.R. Jaffrey, Mol. Cell. 82 (2022) 2236–2251.
[21] J. Li, H. Zhang, H. Wang, Comput. Struct. Biotechnol. J. 20 (2022) 6578–6585.
[22] C. Zhang, G. Jia, Genom. Proteom. Bioinform. 16 (2018) 155–161.
[23] X. Xiong, X. Li, C. Yi, Curr. Opin. Chem. Biol. 45 (2018) 179–186.
[24] S. Ozanick, A. Krecic, J. Andersland, J.T. Anderson, RNA 11 (2005) 1281–1290.
[25] E. Vilardo, C. Nachbagauer, A. Buzet, et al., Nucleic Acids Res. 40 (2012) 11583–11593.
[26] T. Chujo, T. Suzuki, RNA 18 (2012) 2269–2276.
[27] T. Waku, Y. Nakajima, W. Yokoyama, et al., J. Cell Sci. 129 (2016) 2382–2393.
[28] X. Li, X. Xiong, K. Wang, et al., Nat. Chem. Biol. 12 (2016) 311–316.
[29] D. Dominissini, S. Nachtergaele, S. Moshitch-Moshkovitz, et al., Nature 530 (2016) 441–446.
[30] Y. Zhang, L. Lu, X. Li, Exp. Mol. Med. 54 (2022) 1601–1616.
[31] H. Liu, Y. Wang, X. Zhou, RSC Chem. Biol. 3 (2022) 994–1007.
[32] A.S. Felix, A.L. Quillin, S. Mousavi, J.M. Heemstra, Acc. Chem. Res. 55 (2022) 2271–2279.
[33] D. Bartee, S. Thalalla Gamage, C.N. Link, J.L. Meier, Chem. Soc. Rev. 50 (2021) 9482–9502.
[34] J.D. Alfonzo, J.A. Brown, P.H. Byers, et al., Nat. Genet. 53 (2021) 1113–1116.
[35] X.J. You, L. Li, T.T. Ji, et al., Chin. Chem. Lett. 34 (2023) 107181.
[36] Q. Wang, J.H. Ding, J. Xiong, et al., Chin. Chem. Lett. 32 (2021) 3426–3430.
[37] Q.F. Zhang, H.M. Xiao, J.T. Zhan, B.F. Yuan, Y.Q. Feng, Chin. Chem. Lett. 33 (2022) 4746–4749.
[38] B. Chen, B.F. Yuan, Y.Q. Feng, Anal. Chem. 91 (2019) 743–756.
[39] X.M. Tang, T.T. Ye, X.J. You, et al., Chin. Chem. Lett. 34 (2023) 107531.
[40] W.B. Tao, N.B. Xie, Q.Y. Cheng, Y.Q. Feng, B.F. Yuan, Chin. Chem. Lett. 34 (2023) 108243.
[41] S.C. Trewick, T.F. Henshaw, R.P. Hausinger, T. Lindahl, B. Sedgwick, Nature 419 (2002) 174–178.
[42] P.O. Falnes, R.F. Johansen, E. Seeberg, Nature 419 (2002) 178–182.
[43] M. Safra, A. Sas-Chen, R. Nir, et al., Nature 551 (2017) 251–255.
[44] H. Zhou, S. Rauch, Q. Dai, et al., Nat. Methods 16 (2019) 1281–1288.
[45] X. Li, X. Xiong, M. Zhang, et al., Mol. Cell. 68 (2017) 993–1005.e9.
[46] J.H. Ding, C.J. Ma, M.Y. Chen, et al., Anal. Chem. 92 (2020) 2612–2619.
[47] I. Barbieri, T. Kouzarides, Nat. Rev. Cancer 20 (2020) 303–322.
[48] J. Xiong, K.K. Chen, N.B. Xie, et al., Anal. Chem. 94 (2022) 15489–15498.
[49] N.B. Xie, M. Wang, T.T. Ji, et al., Chem. Sci. 13 (2022) 7046–7056.
[50] Y. Wang, J. Wang, X. Li, et al., Nat. Commun. 12 (2021) 6314.